Non-collocated Proprioceptive Sensing for Lightweight Flexible Robotic Manipulators

Xavier Garant, Clément Gosselin *Fellow, IEEE*

***Abstract*—This paper presents the design of a non-collocated feedback system for flexible serial manipulators. The device is a passive serial chain of encoders and lightweight links, mounted in parallel with the manipulator. This measuring arm effectively decouples the manipulator's proprioception from its actuators by providing information on the actual end effector pose, accounting for both joint and link flexibility. The kinematic redundancy of the measuring chain allows for safe operation in the context of human-robot interaction. A simple yet effective error model is introduced to assess the suitability of the proposed sensor system in the context of robotic control. The practicality of the device is first demonstrated by building a physical joint-encoder assembly and a simplified planar measuring arm prototype. With this additional feedback, a task-space position controller is devised and tested in simulation. Finally, the simulation results are validated with an experimental 3-DoF lightweight manipulator prototype equipped with a five-joint measuring arm.**

***Index Terms*—Physical Human-Robot Interaction, Collaborative Robotics, Sensors, Lightweight Robots.**

I. Introduction

IT is a well known fact that the classical manipulator architecture, with collocated proprioceptive sensors and actuators, rapidly faces serious challenges as soon as flexible components are introduced in its structure [1]. This appears as a considerable inconvenience in the context of modern robotic applications. Notably, for the purpose of physical human-robot interaction (pHRI), lightweight (and flexible) robots are desirable for safety reasons.

Indeed, a typical manipulator's only means of measuring its own end effector pose is through the feedback of its actuators' displacement. The pose can theoretically be reconstructed from sensory input, assuming both rigid links and joints. While benign in appearance, this assumption has been guiding robot design for decades. In order for the physical manipulator to conform to this principle, stiffness is one of the prime design criteria. In consequence, the robot must carry additional mass whose sole purpose is to ensure adequate link stiffness. Yet, in the context of interactive applications with humans, mobile mass has been known for some time to carry considerable drawbacks [2]–[4].

To move this mass with precision, stiff actuators with high transmission ratios are required. This comes at the cost of a very high reflected inertia [5] and low bandwidth. One possible improvement is to relocate the motors (which make up a major part of the total mass) at the base of the robot [6]. In recent years, there has also been much research interest in reducing transmission ratios to direct-drive [7] or quasi-direct drive levels [8] to improve the inherent safety of manipulators. At the same time, others have looked into introducing compliance in the manipulator structure to reduce the reflected inertia and reflected stiffness [9].

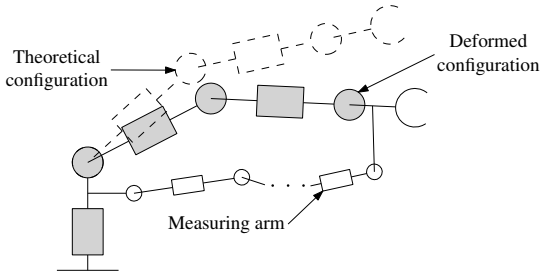

Fig. 1. Schematic representation of a flexible manipulator in a theoretical configuration (dashed white), deformed configuration under load (solid grey) and measuring arm (solid white).

In general, control strategies for flexible manipulators can be divided in two main categories: open-loop model-based control, or closed-loop sensor-based control [1]. In this case, the terms open-loop or closed-loop implicitly refer to whether deflection feedback is used or not. Open-loop control of flexible manipulators has been largely studied and is known to be a complex problem, owing to the very nonlinear and non-minimum phase dynamics [10]–[12]. Thus, this paper focuses on feedback-based approaches to flexible manipulator control.

Common feedback options for deflection sensing in manipulators include strain gauges, accelerometers, and vision systems or range sensors. Strain gauges provide direct information on link deformation, but commonly face challenges related to noise and thermal sensitivity [13]. In addition, strain gauges only measure the local deformation of single *links*, and cannot compensate alone for flexible *joints*. Accelerometers, on the other hand, can provide 'total' deformation information by measuring the acceleration at various points along the manipulator [14]. However, as it is well known, these sensors are also prone to noise and biases, complicating the extraction of position and velocity signals [15]. Finally, vision systems and range sensors can provide precise deflection measurements of both flexible link and flexible joint manipulators [16]. They however come at the cost of additional delays in the control loop and reduced bandwidth, while also requiring more involved calibration methods [17]. Moreover, vision-based control involves additional abstraction layers dedicated to image processing and feature extraction [18].

This work was supported by the *Institut de recherche Robert-Sauvé en santé et en sécurité du travail* (IRSST), the Natural Sciences and Engineering Research Council of Canada (NSERC) and the Canada Research Chair program.

The authors are with the Department of Mechanical Engineering, Université Laval, Québec, QC G1V 0A6, Canada (xavier.garant.1@ulaval.ca, gosselin@gmc.ulaval.ca).

In this paper, a sensor system in the form of a passive measuring arm (as illustrated schematically in Fig. 1) is further developed, with a focus on pHRI applications. The proposed system only relies on encoder signals and therefore does not require computer vision, strain gauges or inertial measurement units. The intent of this system is to provide fast and reliable end effector deflection information, with minimal interference in the interaction between the manipulator and human operator. Using terminology from the closely related field of soft robotics, the proposed sensor system could therefore be considered a 'soft sensor', according to the definition in [19].

Some patents have conceptually explored the idea of adding a measuring arm in parallel between manipulator links [20]–[22], but fall short in regard to the practicality of such an undertaking. One such practical consideration lies in assessing the precision that can be expected from the sensor system. This problem was first tackled mathematically in [23], which found that a simulated measuring arm could theoretically return nanometre level measurements, given very high precision joint encoders. These results were however never experimentally validated and therefore also minimised potential practical pitfalls such as interference between the manipulator and measuring arm, or the combined singularity loci of the integrated robotic unit.

To the best of the author's knowledge, the first and only practical implementation of a measuring arm in the literature was in [24]. Merckaert *et al*. introduced the idea of using tip deflection sensing with the intent to design the manipulator based on strength rather than stiffness. They aptly proved that the deformation can be compensated for, at least in the direction of gravity. They also made a strong case for the safety improvements that this method could yield by reducing the mass of the manipulator. In its current state, however, their sensor system can only tolerate and detect in-plane (2D) tip deflection, thus ignoring out-of-plane forces or torsion inducing moments.

In light of the scarce literature, this paper aims to bring the state of the art on this concept closer to a fully functional and practical sensor system. To this end:

- A basic kinematic structure is proposed for the integrated manipulator-measuring arm unit. Kinematic constraints specific to this application are outlined and design guidelines are provided.
- Kinematic redundancy is leveraged to circumvent otherwise challenging kinematic problems, while also making the device inherently safe for human interaction.
- With its higher degree of freedom (DoF) count, the sensor system is intended to measure the deviation of the robot's end effector pose in all directions.
- A mathematical framework based on differential kinematics is proposed in order to characterise the device's precision. This assessment proves that the pursuit of this design is relevant considering the current technological means and expected orders of magnitude of manipulator reach and payload.

This paper is structured as follows. Section II introduces the proposed kinematic structure of the integrated robotic unit comprising the manipulator and measuring arm. Section III then briefly outlines the forward kinematics of the measuring arm. In Section IV, a mathematical model based on differential kinematics is proposed to assess the precision of the device. Section V discusses the practical requirements and constraints that guide the design process of the physical sensor unit. In Section VI, a practical method is devised to simultaneously assemble and calibrate the unit. A working planar measuring arm prototype is then experimentally validated in Section VII. A position control scheme that takes advantage of the sensor device's feedback is introduced in Section VIII. Section IX then shows simulation results using this controller on a virtual flexible manipulator. Section X presents the design of an integrated robotic unit prototype consisting of a 3-DoF lightweight manipulator equipped with a measuring arm. The experimental validation of this proof of concept is finally discussed in Section XI. Conclusions are drawn in Section XII.

II. Kinematic Architecture

As observed in the literature, in its simplest form, the proposed integrated robotic unit comprises a serial manipulator and a measuring arm extending from the *fixed* base to the end effector of the manipulator, in parallel.

Let us define A and B, the workspace domains of the manipulator and the measuring arm, respectively. Then, in order for the integrated unit to operate freely, the following condition must be met:

$$B \supset A \tag{1}$$

which is more restrictive than what is proposed in [23]. Indeed, in this application, A and B cannot be equal. Practically, the outer limits of B correspond to a singular configuration where the measuring arm is completely extended. Theoretically, in this configuration, external forces would exceptionally be able to generate undesirable internal efforts in the passive measuring arm.

If condition (1) is met, the workspace domain C of the integrated unit is then

$$C = A \cap B \Rightarrow A. \tag{2}$$

However, in order to determine the real usable workspace, the singular domain of the integrated unit must be subtracted from C. The singular domain, noted $\overline{C}$, is given as

$$\overline{C} = \overline{A} \cup \overline{B} \tag{3}$$

where $\overline{A}$ and $\overline{B}$ are the singular domains of the manipulator and measuring arm, respectively.

Additionally, one must also consider the workspace regions that cannot be reached due to interference between the manipulator and measuring arm. Mathematically characterising these interference regions is not trivial.

Concretely, condition (1) also implies that the Cartesian DoF count of the measuring arm must be greater than or equal to the number of DoFs of the manipulator's end effector. However, while this is true in the rigid case, additional conditions apply when considering a flexible manipulator. Indeed, with any number of flexible links and joints, every link along the manipulator can move in six spatial dimensions relative to the

base. Therefore, the number of joints m of the measuring arm must meet the following condition:

$$m \geq 6 - k \tag{4}$$

where k is the number of DoFs allowed by the connection between the tip of the measuring arm and the manipulator's end effector. For instance, a rigid connection would minimally require a 6-joint measuring arm, while a spherical joint connection would minimally require a 3-joint measuring arm, irrespective of the manipulator's architecture. Of course, in this case a spherical connection would only allow the measurement of position deviations, ignoring orientation error.

It is the authors' belief that the aforementioned non-trivial kinematic constraints are one of the main reasons holding back the development of such a sensor system dedicated to flexible manipulators. Therefore, it is proposed to circumvent these issues with the following relaxations:

- In the context of pHRI, minimising moving mass is critical while stationary mass generally does not pose any risk. Therefore, the fixed base link l_0 and first joint j_1 of the manipulator can be made arbitrarily massive, ergo arbitrarily rigid.
- In accordance with the preceding statement, the base of the measuring chain can be attached to the first moving link l_1 of the robot, as close as possible to joint j_1, without compromising accuracy or precision.

The resulting kinematic structure proposed for the integrated robotic unit is graphically represented in Fig. 2. The benefit of this architecture is that it greatly reduces the risk of interference between the manipulator and measuring arm. Indeed, in this case the measuring arm does not span the first joint of the manipulator, which is generally responsible for the largest amplitude movements of the end effector.

To further mitigate the risk of interference, it is also proposed to take advantage of kinematic redundancy. Thus, condition (4) becomes

$$m > 6 - k. \tag{5}$$

This allows the measuring arm to conform to the manipulator in a situation where interference would typically occur. It also virtually prevents the measuring arm from reaching singular configurations, by providing alternative joint arrangements for every Cartesian pose. Moreover and perhaps even more importantly, this grants compliance to the measuring arm when interacting with humans and thus greatly reduces pinching or squeezing risks. The more redundant joints there are, the safer pHRI becomes with the integrated unit, the ideal case being a measuring arm that behaves somewhat like a chain or cable.

III. Forward Kinematics

This section details the forward kinematics of the measuring chain. It is worth noting that for the purpose of controlling a robotic manipulator, the inverse kinematics of the passive measuring arm are irrelevant. Therefore, the inverse kinematics are omitted in this paper.

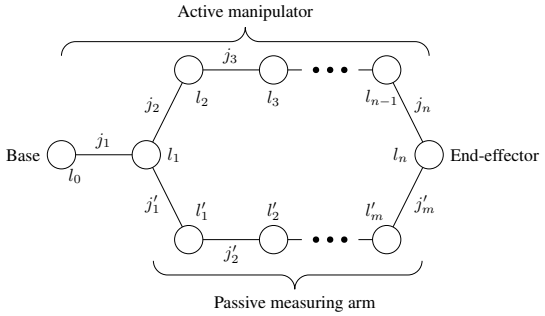

Fig. 2. Graph of the proposed kinematic structure for the robotic unit comprising a manipulator and a measuring arm. Bodies l_i are represented by nodes. Joints j_i are represented by edges.

As a result of the assumptions presented in Section II, the measuring chain's end point position in the fixed reference frame, noted $\mathbf{x}$, can be written as

$$\mathbf{x} = \mathbf{f}_k(\boldsymbol{\theta}, \boldsymbol{\phi}) \tag{6}$$

$$\mathbf{x} = \mathbf{c}_1 + \sum_{i=1}^{m} \mathbf{a}'_i \tag{7}$$

where $\mathbf{f}_k(\boldsymbol{\theta}, \boldsymbol{\phi})$ represents the forward kinematics, $\boldsymbol{\theta}$ is the array of joint positions and $\boldsymbol{\phi}$ stands for the Denavit-Hartenberg (D-H) parameters. Vector $\mathbf{c}_1$ is a slight modification of the classical D-H method and defines the position of the origin of frame $1'$ with respect to frame 1, expressed in the base reference frame (frame 1). Then, following D-H conventions, vector $\mathbf{a}'_i$ defines the position of the origin of frame $i'+1$ with respect to frame i', expressed in frame 1.

IV. Kinematic Sensitivity Error Model

Establishing the error model of a sensor is crucial in assessing its suitability as a feedback device to be used in a control system. In this section, a simple but effective error model is derived, based on well-known serial manipulator equations.

In [23], the following first order Taylor expansion is introduced to model the kinematic error of the measuring arm:

$$\delta\mathbf{x} = \frac{\partial \mathbf{f}_k(\boldsymbol{\theta}, \boldsymbol{\phi})}{\partial \boldsymbol{\theta}} \delta\boldsymbol{\theta} + \frac{\partial \mathbf{f}_k(\boldsymbol{\theta}, \boldsymbol{\phi})}{\partial \boldsymbol{\phi}} \delta\boldsymbol{\phi} \tag{8}$$

where $\delta\mathbf{x}$ is the Cartesian position error and $\delta\boldsymbol{\theta}$ and $\delta\boldsymbol{\phi}$ are the errors on joint coordinates and D-H parameters, respectively. The method in [23] relies on deriving an analytic expression for $\delta\mathbf{x}$ by symbolically differentiating the terms in (8). This process can be tedious and increases in complexity with the number of DoFs, which are expected to be high in the case of the measuring arm.

Joint Error

Clearly, considering the serial architecture of the measuring arm, it can be observed that the first term on the right hand side of (8) is simply equivalent to the product of the Jacobian matrix $\mathbf{J}$ of the measuring arm, and a small joint displacement $\Delta\boldsymbol{\theta}$. Here, $\mathbf{J}$ is defined in the usual sense such that

$$\dot{\mathbf{x}} = \mathbf{J}\dot{\boldsymbol{\theta}} \tag{9}$$

or

$$\Delta \mathbf{x} \simeq \mathbf{J} \Delta \boldsymbol{\theta} \tag{10}$$

for small values of joint displacements $\Delta\boldsymbol{\theta}$ yielding small Cartesian displacements $\Delta\mathbf{x}$.

Moreover, by delving further into differential kinematics, the notion of kinematic sensitivity can be introduced to simplify the error analysis of the measuring arm. Many indices have been proposed in the literature in order to compare the performance of manipulator architectures. However, the kinematic sensitivity index, presented in [25], is of particular interest in the present case because it directly relates to the Cartesian resolution of the measuring chain.

The idea behind this index is to find compatible joint displacements $\Delta\boldsymbol{\theta}$ of unit ∞-norm that yield a global extremum of $\Delta\mathbf{x}$, given equation (10). Writing this problem in terms of dimensionally homogeneous arrays leads to

$$\sigma_{\omega,\infty} = \max_{\|\Delta\boldsymbol{\theta}\|_\infty = 1} \|\mathbf{J}_\omega \Delta\boldsymbol{\theta}\|_\infty = \|\mathbf{J}_\omega\|_\infty \tag{11}$$

$$\sigma_{x,\infty} = \max_{\|\Delta\boldsymbol{\theta}\|_\infty = 1} \|\mathbf{J}_x \Delta\boldsymbol{\theta}\|_\infty = \|\mathbf{J}_x\|_\infty \tag{12}$$

where $\sigma_{\omega,\infty}$ and $\sigma_{x,\infty}$ are the maximum magnitude rotation and displacement, respectively, and

$$\mathbf{J} \equiv \begin{bmatrix} \mathbf{J}_\omega \\ \mathbf{J}_x \end{bmatrix}. \tag{13}$$

Here, $\mathbf{J}_\omega$ and $\mathbf{J}_x$ are the Jacobian sub-matrices respectively associated with the rotational and translational coordinates. These matrices can be numerically computed for any given configuration of the measuring arm.

In fact, any p-norm can be used with this index. However, the ∞-norm is a direct consequence of the common assumption that in any given configuration, the joint displacements $\Delta\boldsymbol{\theta}$ can take any value in an interval bounded by $\pm\Delta\theta_{max}$. This statement is then directly equivalent to

$$\|\Delta\boldsymbol{\theta}\|_\infty \leq \Delta\theta_{max} \tag{14}$$

or

$$\|\Delta\boldsymbol{\theta}\|_\infty \leq 1 \tag{15}$$

with normalised units. Thus, if we consider

$$\Delta\theta_{max} = \sigma_\theta \tag{16}$$

where σ_θ is the encoder resolution in radians, we can extract physical meaning from (11) and (12). Indeed, when multiplying $\sigma_{x,\infty}$ or $\sigma_{\omega,\infty}$ with $\Delta\theta_{max}$, one finds the actual physical maximum rotation and position displacement, respectively Σ_ω and Σ_x, in coherent units:

$$\Sigma_\omega = \sigma_\theta \|\mathbf{J}_\omega\|_\infty \tag{17}$$

$$\Sigma_x = \sigma_\theta \|\mathbf{J}_x\|_\infty \tag{18}$$

This result is effectively equivalent to an upper bound on the Cartesian resolution of the system *in a given configuration*, since its physical interpretation is the maximum allowable end point displacement before any movement is registered by the proprioceptive sensors.

This information can then be used for instance, as a threshold to discriminate significant tip deflections from random noise when operating the robotic unit. Indeed, this method has the advantage that (17) and (18) can easily be numerically computed in real-time. This is also true for more complex kinematic architectures, whereas the method in [23] progressively becomes more involved with a higher DoF count.

While this is considered out of the scope of this paper, if necessary, various approaches can be taken to determine an average or *global* Cartesian resolution of the measuring arm. For instance, one can discretise the entire joint space or a subset of it, and loop over each array of joint values in either a predetermined or randomised fashion. This method however faces the limitation of a rapidly increasing computational cost, with the total number of arrays equal to d^n, where d is the number of discretisations and n is the number of joints. A perhaps more interesting avenue consists in taking into account the fact that the workspace of the measuring arm is constrained by the workspace of the robotic manipulator, plus any significant deformation of the manipulator. Thus, one can discretise the resulting subset of the original measuring arm workspace and compute the inverse kinematics for an arbitrary number of configurations at every selected point.

D-H Parameter Error

To avoid the derivation of the second term in (8), it is possible to measure the actual values of the D-H parameters. Thus, instead of defining manufacturing and assembly tolerances on these dimensions, we can assume their values to either be virtually exact, or having such small error that the second term in (8) is negligible in relation to the first term [23]. One practical method for doing so is presented in Section VI.

V. Sensor System Design

In the following section, the principles guiding the the mechanical and electronic design of the measuring arm are presented.

First and foremost, it is crucial to minimise the mass of the system. This ensures that the measuring arm has a negligible impact on the dynamics of the manipulator.

Second, the form factor of both the encoders and the links of the measuring arm must be small enough to allow adequate mobility. To limit the bulkiness of the system, the size of the joints was limited to a maximum diameter of 30 mm.

Third, the encoders must provide absolute positions. Indeed, because the measuring chain is redundant and its joints are not actuated, the usual process of zeroing incremental encoders by returning to a known configuration is impractical. Furthermore, the sensors must be carefully selected according to their resolution and accuracy. As discussed in Section IV, one can rely on differential kinematics in order to define the required joint resolution as a function of a desired Cartesian resolution.

Fourth, in order to avoid the introduction of delays in the control system, the sampling rate of the measuring arm as a whole must be equal to or greater than 1 kHz. From experience, the authors determined that such a rate is sufficient in the context of real-time control for most robotic applications.

The resulting design, which takes into account all of the above design constraints, is shown in Fig. 3. The joints are

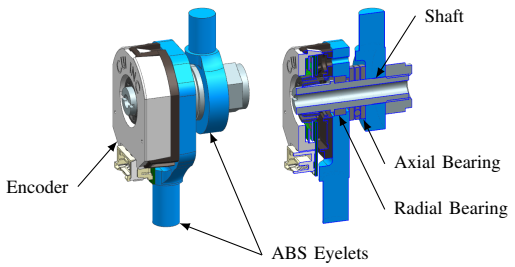

Fig. 3. Design of the joint-encoder assembly. 3D model (left) and section view (right).

made of ABS eyelets sandwiched between radial and axial ball bearings. A small aluminium shaft runs axially through the assembly. The shaft is threaded at one end to pre-constrain the bearings and ensure minimal axial play. The links between the joint assemblies are made of carbon fibre tubes that are bonded to the plastic eyelets. The joint assembly has a mass of 35 g. The carbon fibre tubes have a linear mass of 0.13 g/cm.

Finding commercially available sensors (encoders) that provide sufficient resolution while satisfying the desired form factor is not trivial. The sensors mounted on the joints are CUI AMT-21 14-bit absolute encoders. These encoders provide a good commercial solution with a high resolution relative to their small size. They have a short 100 μs position update time and a fast 2 Mbps communication speed. The encoders communicate over an RS-485 bus. This simplifies cable routing (the bus is comprised of only four wires, power included) and provides basic protection against noise, through differential signalling. The data from all the encoders are collected and processed on the fly through one microcontroller and forwarded to the main CPU in under 300 μs end-to-end, which is fast enough for real-time control.

VI. Build and Calibration

The absolute encoders at each joint of the measuring arm must be calibrated at least once before they can return relevant information. To accomplish this, one practical method is to build an assembly and calibration jig. An example of such a jig is presented in Fig. 4. The jig consists of a metal plate with precisely machined holes into which pegs (precision dowel pins) are inserted. The joints of the measuring arm have through holes centred on their rotation axis with a diameter that matches the pegs. Thus, the joint assemblies can be fitted on the jig with minimal play, in the order of a few microns. Prior to assembly, the relative position of each hole in the jig is measured via a coordinate measuring machine (CMM). This directly translates to precise actual values of D-H parameters. Once the joints are assembled on the jig, carbon fibre tubes, which are used as the links of the measuring arm, are fitted and bonded in place. This completes the building process.

Since the relative position of each joint is known through the CMM measurements, the actual angular position of each joint can be computed. This allows the assembly jig to simultaneously serve as a calibration jig. Indeed, with the measuring arm assembled on the jig in a known configuration, each joint can be zeroed to a known value. This can also prove useful in case of a potential failure after which the measuring arm must be recalibrated.

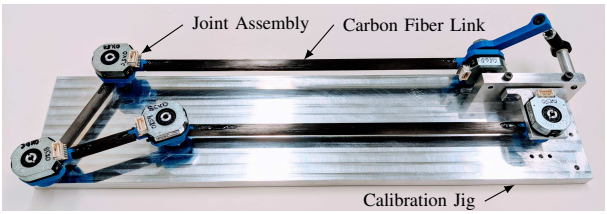

Fig. 4. Example of a 5-joint measuring arm prototype mounted on an assembly and calibration jig.

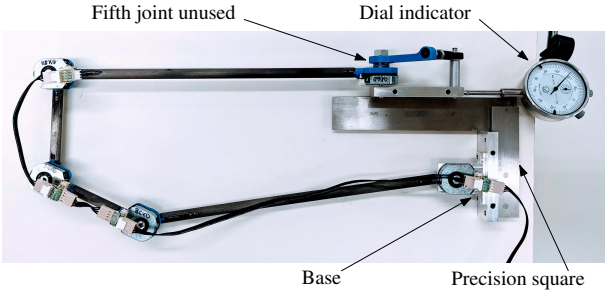

Fig. 5. Experimental setup with functional 4-DoF planar measuring arm (fifth joint unused). The end point is fixed to an aluminium block. The block slides along the precision square, constraining the movement of the end point.

VII. Experimental Validation of the Measuring Arm

In order to validate the practicality of the proposed sensor system concept and construction method, the prototype shown in Fig. 4 was tested against ground truth measurements. Only the first four joints of the prototype were used to measure 2D positions. Thus, with four joints dedicated to a 2D position measuring task, this device has two redundant degrees of freedom. The link lengths of this prototype (in millimetres) are $\{l'_1 \quad l'_2 \quad l'_3 \quad l'_4\} = \{340 \quad 80 \quad 80 \quad 300\}$. These geometric parameters were chosen to match the dimensional order of magnitude of typical manipulators in the 5-7 kg payload range.

The experimental setup is shown in Fig. 5. Concretely, the intent of this setup is to validate that the sensor system can accurately measure position variations. When taking measurements, the displacement of the end point of the kinematic chain is constrained to remain parallel to either the X or Y axis in the base reference frame. To ensure this constraint, the base of the kinematic chain is kept fixed to one edge of a precisely ground machinist square, while the end point is slid by hand along the other edge. During the tests, the redundant DoFs of the measuring arm are unconstrained and the links are free to move on the work surface. The ground truth displacement measurement is given by a plunger type dial indicator, which is also aligned on the precision square. The precision square has a maximum deviation of 0.003 mm, while the dial indicator has a rated accuracy of ± 0.03 mm.

The Cartesian position of the measuring arm's end point is computed using the sensor values and forward kinematics. After each test run, the difference between the final and

TABLE I
EXPERIMENTAL VALIDATION OF THE 4-DOF PLANAR MEASURING ARM

Initial Configuration [deg]	Resolution [mm]	Displacement $\Delta\mathbf{x}$ [mm]		Error Norm [mm]	
	Computed (Max)	Ground Truth	Measured	Absolute	Relative
$\boldsymbol{\theta} = [\ -7.18 \quad 31.23 \quad -122.10 \quad -81.19]^T$	0.42	$[-15.26 \quad 0]^T$	$[-15.4 \quad 0.4]^T$	0.42	0.94%
$\boldsymbol{\theta} = [\ \ 9.58 \quad 104.51 \quad 67.04 \quad -151.60]^T$	0.38	$[\ 22.88 \quad 0]^T$	$[\ 23.1 \quad 0.2]^T$	0.30	0.96%
$\boldsymbol{\theta} = [-77.41 \quad -48.31 \quad -53.39 \quad -90.56]^T$	0.41	$[\ \ 0 \quad 12.70]^T$	$[\ \ 0.1 \quad 12.8]^T$	0.14	0.78%
$\boldsymbol{\theta} = [-93.42 \quad 16.95 \quad -116.04 \quad -76.93]^T$	0.42	$[\ \ 0 \quad 12.70]^T$	$[\ \ 0.2 \quad 12.7]^T$	0.20	0.12%
$\boldsymbol{\theta} = [-92.92 \quad 14.13 \quad -114.32 \quad -76.56]^T$	0.42	$[\ \ 0 \quad 2.54]^T$	$[\ -0.3 \quad 2.4]^T$	0.33	5.02%

initial positions is calculated, yielding the measured end point displacement.

The results are shown in Table I. Five configurations were tested with the indicated measured displacements. The maximum resolution was computed in the initial configuration with the method shown in Section IV. It is worth restating that this number is an upper bound only achievable by considering an extreme case where every joint rotates by up to a full encoder resolution tick, moving the end point in an arbitrary direction. In the actual direction of movement, the precision of the measuring arm is in practice much higher. Still, the maximum resolution remained close to 0.4 mm in each configuration. This sub-millimetre resolution is adequate in the context of pHRI with a flexible manipulator, with expected displacements on the order of a few millimetres to a few centimetres. The measuring arm also proved to be accurate at measuring displacements in the centimetre range, with relative errors under 1%. A small displacement of 2-3 mm showed a slightly higher relative error. This is expected, as a constant uncertainty, such as a resolution error, yields a greater relative difference on a small measurement.

VIII. MODEL-FREE TRAJECTORY TRACKING IN TASK SPACE

With the practicality of the sensor device demonstrated, the next step towards a fully functional robotic unit is the design of a position control scheme. This control scheme must naturally take advantage of the non-collocated feedback of the actual end effector pose provided by the measuring arm.

Consider the general dynamic model of a flexible robotic manipulator:

$$\mathbf{M}(\mathbf{q}_r, \mathbf{q}_f) \begin{bmatrix} \ddot{\mathbf{q}}_r \\ \ddot{\mathbf{q}}_f \end{bmatrix} + \mathbf{h}(\mathbf{q}_r, \mathbf{q}_f, \dot{\mathbf{q}}_r, \dot{\mathbf{q}}_f) + \mathbf{g}(\mathbf{q}_r, \mathbf{q}_f) + \mathbf{K}(\mathbf{q}_r, \mathbf{q}_f) \begin{bmatrix} \mathbf{q}_r \\ \mathbf{q}_f \end{bmatrix} = \begin{bmatrix} \boldsymbol{\tau}_m \\ \mathbf{0} \end{bmatrix} \quad (19)$$

where $\mathbf{q}_r$ is the vector of joint variables ('rigid' coordinates), $\mathbf{q}_f$ is the vector of deformation variables, $\mathbf{M}$ is the generalised inertia matrix, $\mathbf{h}$ is the vector of Coriolis and centrifugal terms, $\mathbf{g}$ is the vector of gravitational terms, $\mathbf{K}$ is the stiffness matrix of the system, and $\boldsymbol{\tau}_m$ is the vector of actuator torques applied at the joints.

The objective is to find a time-varying torque input $\boldsymbol{\tau}_m$ such that the actual pose of the manipulator, noted $\mathbf{x}_f$, converges to the desired task space pose $\mathbf{x}_d$. However, while the values of $\mathbf{q}_r$ and $\dot{\mathbf{q}}_r$ are given by the motor encoders, the values of $\mathbf{q}_f$ are unknown. Thus, the actual end effector pose of the flexible manipulator, given by

$$\mathbf{x}_f = \mathbf{f}(\mathbf{q}_r, \mathbf{q}_f) \quad (20)$$

cannot be computed. Instead, the pose of the flexible manipulator is measured, such that

$$\mathbf{x}_f = \mathbf{x} \quad (21)$$

where $\mathbf{x}$ is given by the measuring arm according to (7).

The proposed trajectory tracking control is a simple modification of a typical collocated proportional-derivative (PD) controller where the desired task space poses and their time derivatives are mapped to joint coordinates. Thus, the controller equation is given by

$$\boldsymbol{\tau}_m = \mathbf{G}_P \mathbf{J}_r^{-1}(\mathbf{q}_r)[\mathbf{x}_d - \mathbf{x}_f] + \mathbf{G}_D[\mathbf{J}_r^{-1}(\mathbf{q}_r)\dot{\mathbf{x}}_d - \dot{\mathbf{q}}_r] + \mathbf{g}_r(\mathbf{q}_r) \quad (22)$$

where $\mathbf{G}_P$ and $\mathbf{G}_D$ are, respectively, the proportional and derivative gain matrices and $\mathbf{J}_r(\mathbf{q}_r)$ and $\mathbf{g}_r(\mathbf{q}_r)$ are, respectively, the Jacobian matrix and the vector of gravity compensation torques, both associated with the rigid body model of the flexible manipulator. As such, the controller does not rely on prior knowledge of the dynamic model of the manipulator, nor its stiffness matrix.

Alternatively, if velocity control is used instead of torque or current control, a close equivalent to (22) can be achieved with

$$\dot{\mathbf{q}}_{r,c} = \mathbf{J}_r^{-1}(\mathbf{q}_r)[\dot{\mathbf{x}}_d + \boldsymbol{\lambda}(\mathbf{x}_d - \mathbf{x}_f)] \quad (23)$$

where $\dot{\mathbf{q}}_{r,c}$ is the actuator velocity command sent to the controller and $\boldsymbol{\lambda}$ is a tuning parameter matrix.

As expected with this type of Cartesian controller, extra caution is required in the vicinity of the singular configurations of the manipulator, due to the bad conditioning of the Jacobian matrix. Nevertheless, there exist many methods that circumvent this issue, with a notable example being the damped least squares method [26].

IX. SIMULATION

As a first step towards demonstrating the effectiveness of the proposed solution, a dynamic simulation was carried out in MATLAB. The simulated robot is a 2-DoF planar serial manipulator with flexible rotary joints subject to gravity. The parameters of the simulated manipulator are shown in Table II.

This simulation is a three step process. First, a trajectory planner generates the next desired pose according to the

TABLE II
SIMULATED MANIPULATOR PARAMETERS

Parameter	Value
Link 1 Length [m]	0.45
Link 2 Length [m]	0.45
Link 1 Mass [kg]	1.44
Link 2 Mass [kg]	0.50
Payload Mass [kg]	2
Joint 1 Reduction ratio	121:1
Joint 2 Reduction ratio	90:1
Joint 1 Moment of inertia* [kgm^2]	2.5×10^{-3}
Joint 2 Moment of inertia* [kgm^2]	1.0×10^{-3}
Joint 1 Stiffness [Nm/rad]	2000
Joint 2 Stiffness [Nm/rad]	1000

* At reducer input.

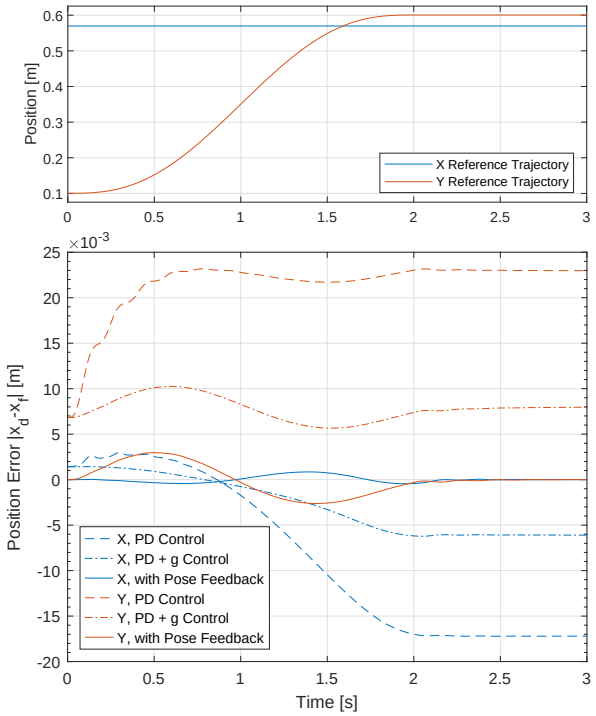

Fig. 6. Desired reference trajectories in task space and tracking error of three different controllers applied to the simulated flexible manipulator. Payload is 2 kg and gravity is in the negative Y direction.

specified trajectory. Second, the time-varying torque inputs are computed according to the controller equation and using the manipulator's current kinematic states. Third, the dynamic model in (19) is numerically solved, yielding the next kinematic states.

The task consists in moving up 0.5 meters in the Y direction (against gravity) following a fifth order interpolation, while keeping the X coordinate fixed. The trajectory is executed in 2 seconds. The graphs in Fig. 6 show the desired reference trajectory and the resulting tracking error of three different controllers applied to this task. The relevant error values for quantitative analysis are presented in Table III.

The first case illustrates the results of a traditional PD controller which ignores the robot's flexibility. In other words, this controller relies on the rigid model, forward kinematics and actuator positions of the manipulator to track its end effector

TABLE III
SIMULATION TRACKING ERROR RESULTS

	Error Norm [mm]				
Controller	Initial	Final	Min	Max	RMS
PD	7.0	28.7	7.0	28.8	24.8
PD + g	7.0	10.0	6.4	10.3	8.9
Pose Feedback	0	0	0	3.0	1.6

pose. As expected, there is a non-negligible initial error in the direction of gravity, due to flexibility, which worsens as the manipulator reaches a more extended configuration. Because of the coupled nature of the serial manipulator, a notable error in the X direction is also observed. Practically, the actual manipulator stands lower than predicted by the rigid model, deformed under the weight of its own links and its payload. This static error, expected with PD control, is worsened by the flexibility of the manipulator. Thus, the trajectory is not accurately tracked and its end point is never reached.

The second case shows the effect of including a feedforward gravity compensation term, based on the rigid static model, in the PD control scheme ('PD + g' control). As expected, although every error metric is improved compared to the PD controller, a large static error of 10 mm remains in the final configuration. Gravity compensation cannot adequately eliminate the static error of the PD controller without the stiffness model of the manipulator. Indeed, in this case, once the forward kinematics –based on the actuator positions– have converged to the desired pose, the controller lacks the necessary information to further adjust the actual pose of the manipulator. In this sense, including an integrator term in this controller would also be useless.

The third case illustrates the behaviour of the proposed controller with actual pose feedback, as defined in (22). This additional feedback is considered available at each time step of the simulation, since the real sensor system allows sampling rates higher than 1 kHz. The results clearly show that the actual pose of the flexible manipulator converges to the desired value, both statically and dynamically. The static error tends to zero in the final configuration. In this example, the maximal error magnitude, which occurs during the most dynamic phases of the trajectory, is 3 mm. This is lower than the overall minimum error achieved with the other controllers. Thus, the end effector effectively tracks the prescribed Cartesian trajectory.

The simulation results indicate that, in theory, the deformation of a flexible manipulator can be compensated by feeding back the measurement of the end effector pose. Moreover, with this type of feedback, the controller does not require a detailed dynamic model of the robot. Of course, this simulation represents an idealized model of a flexible joint manipulator and ignores practical considerations such as noise, delays, friction, or bending of the links. Therefore, the next sections are aimed at introducing and detailing an experimental setup to fully validate the proposed solution in real-world conditions.

X. PROOF OF CONCEPT

As discussed in the Introduction, the proposed sensor system can shift the design paradigm of robotic manipulators for

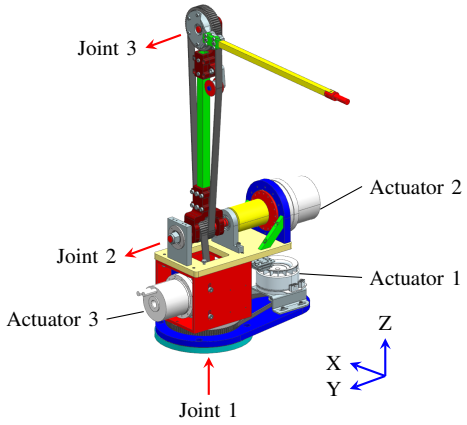

Fig. 7. CAD model of the 3-DoF lightweight serial manipulator prototype. Joint axes are indicated with red arrows.

certain applications such as pHRI. Indeed, with proprioception decoupled from actuation, the design can be based on strength, rather than stiffness. To substantiate this claim, a serial manipulator prototype (shown in Fig. 7) was built. With three rotary joints, this manipulator was designed for 3D positioning tasks, with a maximum payload of 5 kg and a reach of 0.9 m. The prototype was deliberately made flexible, for practical and demonstration purposes.

Practically, positioning the distal actuator at the base of the robot rather than at the joint requires a means of power transmission. Again, moving the actuators to the base has the advantage of drastically reducing the moving mass and inertia of the robot. However, due to the manipulator links being flexible, 'rigid' power transmission methods such as drive shafts or gear trains are inadequate. Indeed, the method must accommodate some degree of deflection in the links. With such constraints, synchronous pulleys and belts are a natural lightweight and low-backlash solution. These belts are inherently flexible and this property is generally only negligible for short belt lengths or very stiff materials. In consequence, the rotational stiffness of the affected joint is effectively reduced.

For demonstration purposes, the second and third manipulator links were designed as slender as possible. With this methodology, the links can still withstand the static and dynamic efforts induced by the payload, but are more flexible than links whose mass would be distributed away from the centroid of their cross-section. Moreover, a flexible coupling was chosen to transmit power to the second joint, rather than rigidly attaching the second link to the actuator. Finally, per the reasoning detailed in Section II, the first mobile link and the first joint were designed to be rigid.

The rotational stiffness of the second joint is mainly determined by the flexible coupling between the actuator and the link. The selected coupling is specified at a static torsional stiffness of 2600 Nm/rad. The stiffness of the third joint is governed by the type of belt, its section properties, and its total length. Computing and transforming the linear stiffness of the belt to a static torsional stiffness yields a value in the order of 1300 Nm/rad at the distal joint (joint 3). For comparison,

TABLE IV
MASS PROPERTIES OF THE PROTOTYPE VERSUS A UR5 ROBOT

Property	Link	Prototype	UR5 Robot
Mass [kg]	l_1	9.90	3.70
	l_2	1.44	8.39
	l_3	0.50	2.33
Moment of inertia* [kgm^2]	l_1	0.182	0.008
	l_2	0.077	0.597
	l_3	0.014	0.101

* Moment of inertia of link l_i is given about joint j_i.

values around 10^5 Nm/rad represent a minimum level of elasticity that can be neglected in practice [27]. Finally, the second and third links were designed to each allow a deflection of up to two centimetres in the direction of gravity when in the least favourable (horizontal, fully extended) configuration.

This manipulator is *not* equipped with link side encoders. Thus, with flexible links and flexible joints, the manipulator alone cannot accurately estimate its actual pose. The encoders are integrated into the actuators for joint control purposes. The first actuator is a Maxon EC-90 direct drive motor coupled to a 4.54:1 synchronous belt reducer. The second actuator is a Harmonic Drive SHA-25 with a 121:1 integrated gearbox. The third actuator is a Harmonic Drive SHA-20 with a 81:1 built-in reducer coupled to a synchronous belt transmission, yielding an effective ratio of 90:1 at the third joint.

The resulting mass properties of the prototype, given by the CAD model, are shown in Table IV, along with values from the Universal Robots UR5 manipulator for comparison. The UR5 cobot is ubiquitous in industry and in the literature and was thus chosen for comparison. Its parameters are also typical of manipulators in the 5 kg payload range. As expected, for a similar payload and reach, the proposed design allows the moving mass (links 2 and 3) to be drastically reduced. When combined with the lower moment of inertia of the links, a much lower reflected inertia at the end-effector can be expected. For instance, the total moment of inertia of the robot about joint 1 in a completely extended horizontal configuration is 0.446 kgm^2 for the proposed prototype and 1.846 kgm^2 for the UR5. Moreover, while the mass of the first link is naturally greater, the total mass is notably reduced. Of course, when comparing values, it should be considered that a UR5 is designed to carry the weight of 3 other links and actuators further down the kinematic chain. This however only further supports the idea that these actuators should ideally be moved as close to the base as possible.

Along with the manipulator prototype, an associated measuring arm was also designed and built, according to the methods in Section V and Section VI. The actual device and a schematic representation of its kinematic model are shown in Fig. 8. The complete robotic unit is also shown in a working configuration in Fig. 9. As it can be observed, this measuring arm is different from the planar model that was introduced in Section VII for testing purposes. For simplicity, the number of joints was limited to five. Along the kinematic chain, each joint axis is perpendicular to the previous joint, yielding a potential of five Cartesian DoFs. However, the end point of

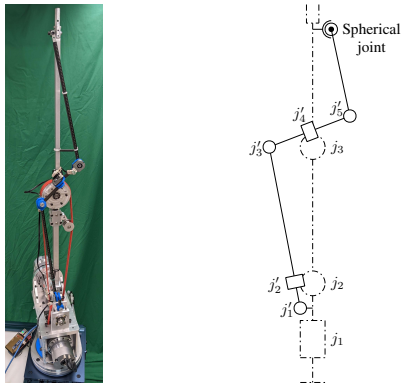

Fig. 8. (Left) Parallel measuring arm mounted on serial manipulator prototype. (Right) Schematic representation of the manipulator (dashed lines) and measuring arm (solid lines).

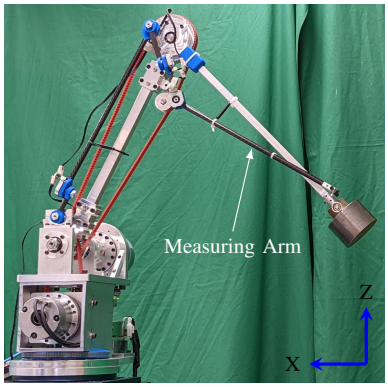

Fig. 9. Robotic unit prototype in working configuration with 2 kg payload.

TABLE V
STATIC DEFLECTION OF THE MANIPULATOR AT THE END EFFECTOR WHEN ADDING A 2 KG PAYLOAD WITH BRAKES APPLIED

Joint Configuration [deg]	Deviation [mm]
$\mathbf{q} = [0 \quad 0 \quad 90]^T$	10.0
$\mathbf{q} = [0 \quad 40 \quad 80]^T$	14.5
$\mathbf{q} = [0 \quad 80 \quad 5]^T$	15.0

the measuring chain is connected to the end effector of the manipulator by a spherical joint, restricting the number of Cartesian DoFs to three. Thus, this specific model of the proposed sensor system is designed to only measure the 3D position (not the orientation) of the end effector. As a result, as explained in Section II, this measuring arm has two redundant joints which allow link movements without affecting the measured value. Due to this relatively low degree of redundancy, elastic elements are used to maintain the measuring arm in a favourable configuration close to the manipulator.

In order to provide a better picture of the overall flexibility of the robot, Table V shows the measured deflection at the end-effector in three typical configurations with a 2 kg payload. To collect the data, the manipulator is first put into the desired configuration with the actuator brakes applied and without a payload. This initial unloaded position is recorded by the measuring arm. The payload is then added and the new static equilibrium position is recorded by the measuring arm. With the brakes applied, the motor side of the joints cannot move and the deflection can only be a result of the flexibility of the joints and links. It is worth noting that this method only measures the deflection caused by the payload. Indeed, before adding the payload, the manipulator is already slightly deformed under its own weight. The first configuration has the second and third link respectively vertical and horizontal. The second configuration has both links at an angle in a typical working configuration, where the work surface would be at base height. The third configuration has the manipulator almost completely extended horizontally.

XI. EXPERIMENTAL VALIDATION

The final step in validating the proposed sensor system consists in testing it on an actual robotic task. To this end, two trajectory tracking tasks are carried out in real-world conditions with the physical integrated robotic unit described in Section X. Both trajectories require active error compensation in every coordinate. The actual Cartesian position of the manipulator is tracked by the measuring arm.

The relevant experimental results for both trajectories are summarised in Table VI. The reported uncertainty in the table is computed by converting the resolution of the encoders to standard uncertainty and using the method shown in Section IV.

Fig. 10 shows the test results for the same trajectory as in Section IX. Practically, the manipulator must move a 2 kg payload 500 mm up in the Z direction (against gravity) in 2 seconds. It is interesting to note that with traditional PD control, unintuitive out-of-plane deflections (in the Y direction) can not only be observed in the initial configuration, but become larger in the less favourable (more extended) final configuration. This phenomenon was not observable in the 2D simulation. Still, as expected, the main components of the position error are caused by the very large in-plane (XZ) deflections, which reach their maximum value around the point of maximum velocity. The results with the proposed sensor system show a drastic reduction in both static and dynamic errors. Indeed, even in the unfavourable final configuration, the out-of-plane static error is virtually eliminated with respect to the precision of the prototype sensor, and the in-plane static errors are reduced to under 0.4 mm, for a total error norm of 0.5 mm. The maximum dynamic error in this example trajectory is reduced by 58% compared to the traditional PD approach. The remaining dynamic error could be further reduced by including inertia feedforward terms (computed torque method) in the controller or, naturally, by considering trajectories with lower dynamics.

Fig. 11 shows the time graphs of the second trajectory. This trajectory requires coordinated motion of the three actuators and illustrates the behaviour of the robot when moving perpendicularly to gravity. Practically, the manipulator must move a 2 kg payload 400 mm sideways in the Y direction (side to side and not front to back) in 2 seconds. All three coordinates show very low error when using pose feedback compared to the traditional PD controller. While the final configuration differs from the first experiment, the static error is again reduced to

TABLE VI
EXPERIMENTAL TRACKING ERROR RESULTS

		Error Norm [mm]					$\pm 1\sigma$ Uncertainty [mm]		
Trajectory	**Controller**	Initial	Final	Min	Max	RMS	Initial	Final	Average
Vertical	Pose Feedback	0.3	0.5	0.2	8.4	4.3	± 0.13	± 0.16	± 0.15
	PD + g	9.2	17.4	9.0	20.0	16.8			
Horizontal	Pose Feedback	0.3	0.5	0	2.9	1.2	± 0.14	± 0.14	± 0.14
	PD + g	11.5	11.2	9.1	11.6	10.8			

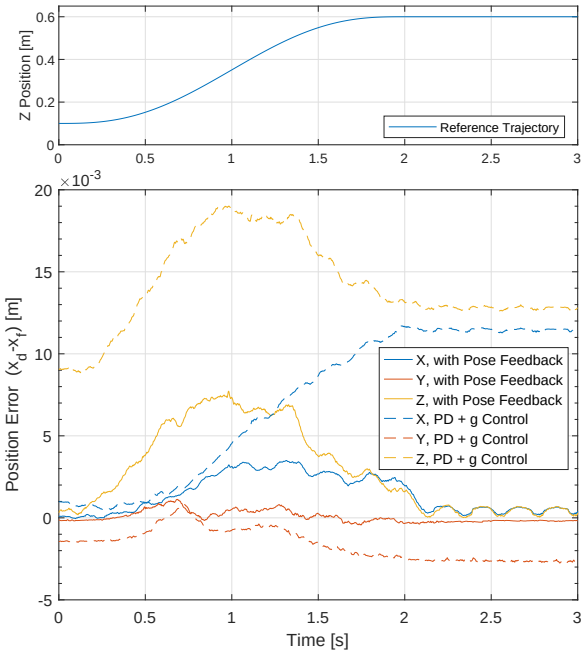

Fig. 10. (Top) Prescribed vertical trajectory in task space, where $x_d = -0.5$ m and $y_d = 0.03$ m are constant. (Bottom) Position error during the trajectory tracking task, with the proposed control and with a PD control with gravity compensation (PD + g). Payload is 2 kg and gravity is in the negative Z direction.

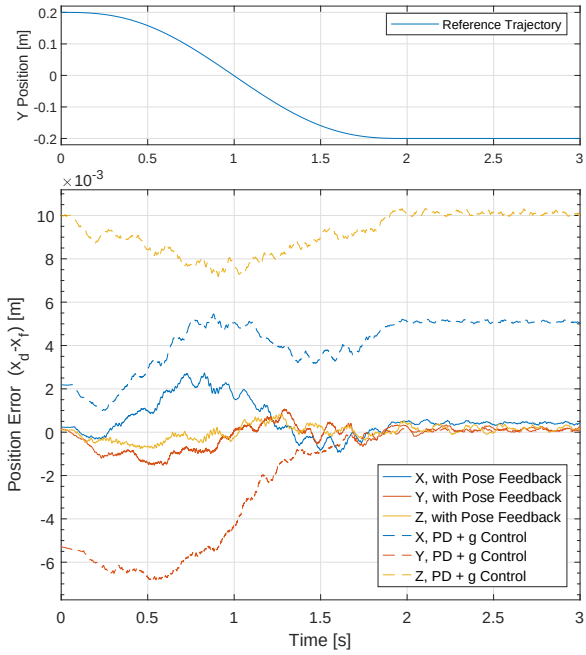

Fig. 11. (Top) Prescribed horizontal trajectory in task space, where $x_d = -0.3$ m and $z_d = 0.4$ m are constant. (Bottom) Position error during the trajectory tracking task, with the proposed control and with a PD control with gravity compensation (PD + g). Payload is 2 kg and gravity is in the negative Z direction.

0.5 mm, a notable improvement over the 11.2 mm error with PD control.

To conclude, these results indicate that:

1) The proposed sensor system and controller effectively compensate the static deflection of a flexible manipulator. These results align with what is reported in [24], where a similar vertical static error component of 0.3 mm was achieved (with a simpler 2-DoF flexible manipulator with a 45% smaller reach) and shown to be better than a commercial KUKA robot arm.
2) While doing so, we have also effectively expanded the concept to non-trivial multi-DoF error measurement and compensation, along with dynamic trajectory tracking.

XII. CONCLUSION

In this paper, a non-collocated sensor system consisting of a serial chain of lightweight links and instrumented passive joints was developed. This device is mounted in parallel to a flexible robotic manipulator to form an integrated robotic unit that can measure its own deflection at the end effector. The kinematic constraints associated with the device were detailed and shown to be considerable design obstacles. To avoid these obstacles, a basic kinematic structure was proposed where the measuring arm spans all but the first link and joint of the manipulator. It was also proposed to take advantage of kinematic redundancy in the measuring arm to prevent any interference with the manipulator, while also ensuring the safety of human operators. To assess the precision of this sensor system, an error model was developed based on a kinematic sensitivity index. This method gives an upper bound on the Cartesian resolution of the device in a given configuration. A simple mechanical and electronic design, which allows the device to be easily assembled and calibrated, was presented. The practicality of the measuring arm was first demonstrated by comparing actual measurements from a simplified planar prototype against ground truth values. Then, with feedback on the actual end effector pose readily available, a position control scheme was devised. The controller allows a flexible manipulator to track trajectories in task space without a dynamic model or a stiffness model, as shown by simulation

results. Finally, a complete integrated robotic unit was built as an experimental setup. The unit comprises a lightweight 3-DoF manipulator and a 5-DoF redundant measuring arm. The experimental results indicate that the robot can effectively compensate position errors and accurately track trajectories even with flexible links and joints.

Such a sensor system introduces new possibilities for applications related to pHRI. Concretely, the detection of user-induced deviations at the end effector will be investigated in future works. This could lead to new control possibilities based on intuitive physical interactions between the human operator and the robot.

REFERENCES

[1] C. T. Kiang, A. Spowage, and C. K. Yoong, "Review of Control and Sensor System of Flexible Manipulator," *Journal of Intelligent & Robotic Systems*, vol. 77, no. 1, pp. 187–213, jan 2015.

[2] S. Haddadin, A. Albu-Schaffer, and G. Hirzinger, "The role of the robot mass and velocity in physical human-robot interaction - Part I: Non-constrained blunt impacts," in *2008 IEEE International Conference on Robotics and Automation*. IEEE, may 2008, pp. 1331–1338.

[3] S. Haddadin and E. Croft, "Physical Human–Robot Interaction," in *Springer Handbook of Robotics*, O. Siciliano Bruno and Khatib, Ed. Cham: Springer International Publishing, 2016, pp. 1835–1874.

[4] T. Steinecker, A. Kurdas, N. Mansfeld, M. Hamad, R. J. Kirschner, S. Abdolshah, and S. Haddadin, "Mean Reflected Mass: A Physically Interpretable Metric for Safety Assessment and Posture Optimization in Human-Robot Interaction," in *2022 International Conference on Robotics and Automation (ICRA)*. IEEE, may 2022, pp. 11 209–11 215.

[5] P. L. García, S. Crispel, E. Saerens, T. Verstraten, and D. Lefeber, "Compact Gearboxes for Modern Robotics: A Review," *Frontiers in Robotics and AI*, vol. 7, p. 103, aug 2020.

[6] A. De Santis, B. Siciliano, A. De Luca, and A. Bicchi, "An atlas of physical human–robot interaction," *Mechanism and Machine Theory*, vol. 43, no. 3, pp. 253–270, mar 2008.

[7] K. Wen, T. S. Nguyen, D. Harton, T. Laliberte, and C. Gosselin, "A Backdrivable Kinematically Redundant (6+3)-Degree-of-Freedom Hybrid Parallel Robot for Intuitive Sensorless Physical Human-Robot Interaction," *IEEE Transactions on Robotics*, vol. 37, no. 4, pp. 1222–1238, aug 2021.

[8] D. V. Gealy, S. McKinley, B. Yi, P. Wu, P. R. Downey, G. Balke, A. Zhao, M. Guo, R. Thomasson, A. Sinclair, P. Cuellar, Z. McCarthy, and P. Abbeel, "Quasi-direct drive for low-cost compliant robotic manipulation," *Proceedings - IEEE International Conference on Robotics and Automation*, vol. 2019-May, pp. 437–443, may 2019.

[9] S. Toxiri, A. Calanca, J. Ortiz, P. Fiorini, and D. G. Caldwell, "A Parallel-Elastic Actuator for a Torque-Controlled Back-Support Exoskeleton," *IEEE Robotics and Automation Letters*, vol. 3, no. 1, pp. 492–499, jan 2018.

[10] R. H. Cannon and E. Schmitz, "Initial Experiments on the End-Point Control of a Flexible One-Link Robot," *The International Journal of Robotics Research*, vol. 3, no. 3, pp. 62–75, sep 1984.

[11] M. Sayahkarajy, Z. Mohamed, and A. A. Mohd Faudzi, "Review of modelling and control of flexible-link manipulators," *Proceedings of the Institution of Mechanical Engineers, Part I: Journal of Systems and Control Engineering*, vol. 230, no. 8, pp. 861–873, sep 2016.

[12] T. Berger and L. Lanza, "Output tracking for a non-minimum phase robotic manipulator," *IFAC-PapersOnLine*, vol. 54, no. 9, pp. 178–185, 2021.

[13] D. Feliu-Talegon and V. Feliu-Batlle, "Control of Very Lightweight 2-DOF Single-Link Flexible Robots Robust to Strain Gauge Sensor Disturbances: A Fractional-Order Approach," *IEEE Transactions on Control Systems Technology*, 2021.

[14] P. Staufer and H. Gattringer, "State estimation on flexible robots using accelerometers and angular rate sensors," *Mechatronics*, vol. 22, no. 8, pp. 1043–1049, dec 2012.

[15] D. Subedi, T. N. Aune, I. Tyapin, and G. Hovland, "Static Deflection Compensation of Multi-Link Flexible Manipulators Under Gravity," *IEEE Access*, vol. 10, pp. 9658–9667, 2022.

[16] M. Hussein, "A review on vision-based control of flexible manipulators," *Advanced Robotics*, vol. 29, no. 24, pp. 1575–1585, dec 2015.

[17] J. Oliveira, A. Ferreira, and J. C. Reis, "Design and experiments on an inflatable link robot with a built-in vision sensor," *Mechatronics*, vol. 65, p. 102305, feb 2020.

[18] U. K. Sahu, D. Patra, and B. Subudhi, "Vision-based tip position tracking control of two-link flexible manipulator," *IET Cyber-Systems and Robotics*, vol. 2, no. 2, pp. 53–66, jun 2020.

[19] A. Chen, R. Yin, L. Cao, C. Yuan, H. Ding, and W. Zhang, "Soft robotics: Definition and research issues," in *2017 24th International Conference on Mechatronics and Machine Vision in Practice (M2VIP)*. IEEE, nov 2017, pp. 366–370.

[20] J. P. W. Flemming, "Monitoring the location of a robot hand," U.S. Patent 4 119 212A, 7 18, 1977.

[21] A. H. Slocum, "Mechanism to determine position and orientation in space," U.S. Patent 4 606 696A, 6 25, 1984.

[22] A. Grädener and L. Rokeach, "Arrangement for an articulated arm robot and method for determining the positioning of a mount for an end effector of an articulated arm robot," International Patent WO2 019 011 381A1, 1 17, 2019.

[23] S. Gong, "A novel ultra-precision integrated robotic system," *Robotica*, vol. 23, no. 4, pp. 501–513, jul 2005.

[24] K. Merckaert, A. De Beir, N. Adriaens, I. El Makrini, R. Van Ham, and B. Vanderborght, "Independent load carrying and measurement manipulator robot arm for improved payload to mass ratio," *Robotics and Computer-Integrated Manufacturing*, vol. 53, pp. 135–140, oct 2018.

[25] P. Cardou, S. Bouchard, and C. Gosselin, "Kinematic-sensitivity indices for dimensionally nonhomogeneous jacobian matrices," *IEEE Transactions on Robotics*, vol. 26, no. 1, pp. 166–173, feb 2010.

[26] S. R. Buss and J.-S. Kim, "Selectively Damped Least Squares for Inverse Kinematics," *Journal of Graphics Tools*, vol. 10, no. 3, pp. 37–49, jan 2005.

[27] L. Zollo, B. Siciliano, A. De Luca, E. Guglielmelli, and P. Dario, "Compliance Control for an Anthropomorphic Robot with Elastic Joints: Theory and Experiments," *Journal of Dynamic Systems, Measurement, and Control*, vol. 127, no. 3, pp. 321–328, sep 2005.

Xavier Garant received the B.Eng. degree and the M.Sc. degree in Mechanical Engineering from Université Laval, Québec, Canada, in 2017 and 2019, respectively. He was a visiting student at the Institute of Robotics and Mechatronics of the DLR in Oberpfaffenhofen, Germany, in 2019. He is currently working towards the Ph.D. degree in Mechanical Engineering at the *Laboratoire de robotique*, Department of Mechanical Engineering, Université Laval. His research revolves around robotics and dynamics, with a special interest in the modelling, design and control of complex robotic systems.

Clément Gosselin (FIEEE, FASME, FRSC) received the Ph.D. degree from McGill University, Montréal, Canada in 1988. He was then a post-doctoral fellow at INRIA in Sophia-Antipolis, France. In 1989 he was appointed by the Department of Mechanical Engineering at *Université Laval*, Québec where he is a full professor since 1997 and where he held the Canada Research Chair in Robotics and Mechatronics from 2001 to 2021. He was a visiting researcher at the RWTH in Aachen, Germany, at the University of Victoria and at the IRCCyN in Nantes, France. He has directed many research initiatives, including collaborations with several Canadian and foreign high-technology companies and he has trained more than 130 graduate students. He is the author of numerous publications, several patents and two books. His research interests include the kinematics and dynamics of parallel manipulators, the development of human-friendly robots and haptic devices and the mechanics of grasping.